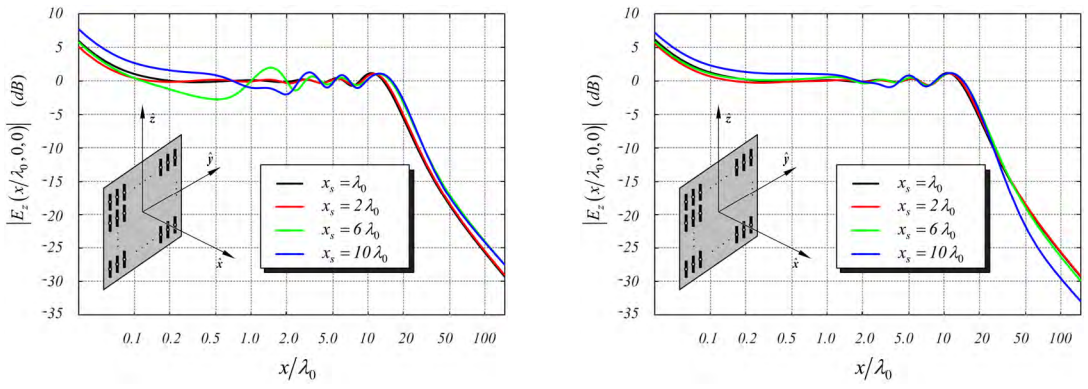

FIGURE 5. Bessel beam electric field magnitude ($z-$component) along the $x-$axis for different x_S synthesis planes. (a) synthesis on open surface, (b) synthesis on closed surface, obtained using modal filtering. Field synthesis on closed surfaces exhibits less ripple than for synthesis on open surfaces, which are characterized by more pronounced yet limited amplitude ripple.

TABLE 3. Performance metrics for Bessel beams synthesis for target areas located at several distances from the array.

E-Field Synthesis (*Unfiltered*) - CLOSED SYNTHESIS SURFACE					
x_s	$NMSE_{open}$	$\eta_{rad_{open}}$	$NMSE_{closed}$	$\eta_{rad_{closed}}$	P_{in}
λ_0	-23.5 dB	86.3%	-22.9 dB	86.3%	0.916mW
$2\lambda_0$	-20.0 dB	87.3%	-19.4 dB	87.4%	0.899 mW
$6\lambda_0$	-12.1 dB	83.6%	-11.3 dB	84.3%	0.878 mW
$10\lambda_0$	-8.0 dB	82.5%	-7.3 dB	83.9%	0.786 mW
E-Field Synthesis (*Filtered with* $10^{-3}\,\lambda_{\max}$) - OPEN SYNTHESIS SURFACE					
λ_0	-23.3 dB	86.4 %	-22.7 dB	86.4 %	0.916 mW
$2\lambda_0$	-20.2 dB	86.8 %	-18.5 dB	87.2%	0.907 mW
$6\lambda_0$	-13.7 dB	42.0 %	0.9 dB	79.9 %	1.825 mW
$10\lambda_0$	-9.4 dB	38.6 %	2.2 dB	81.4%	1.874 mW

the corresponding Bessel beams moving away orthogonally from the array is reported in Fig. 5, for the case of filtered synthesis performed on open and closed surfaces. In both cases the field propagation is essentially tubular up and until the transition towards the spherical wave propagation regime. Smaller ripple is indeed observed in the case of field synthesis performed on closed surfaces.

Tables 1 and 2 also list the realized radiation efficiency $\eta_{rad_{closed}}$, the radiation efficiency $\eta_{rad_{open}}$ relative to the target Bessel beam surface, as well as the incident power P_{in} required collectively at the array ports. All these quantities present quite stable values for closed-surface synthesis, but they may swing widely in the case of open-surface synthesis. From a designer's viewpoint, the closed-surface technique appears to be more attractive due to less demanding dynamical range requisites for the RF circuitry, although its numerical implementation may require evaluating the array field on large domains, especially for distant target areas.

In many practical cases, only the electric (or the magnetic) field distribution needs to be assigned. For instance, this may be the case in applications dealing with electric field synthesis or focusing without any constraint on the corresponding magnetic field (short range communications, heating of lossy materials, etc.). In these instances, the so-called

TABLE 4. NMSE error (closed surface) in presence of a Gaussian dispersion of the excitation profile magnitudes (E-H-field synthesis filtered with threshold $10^{-3}\lambda_{max}$).

	$x_s = 0.5\lambda_0$		$x_s = \lambda_0$		$x_s = 2\lambda_0$		$x_s = 6\lambda_0$		$x_s = 10\lambda_0$	
	MV (dB)	SD (dB)	MV (dB)	SD (dB)	MV (dB)	SD (dB)	MV (dB)	SD (dB)	MV (dB)	SD (dB)
$\sigma_{Mag} = 0\,dB$	-21.8	-	-22.8	-	-19.4	-	-11.2	-	-7.3	-
$\sigma_{Mag} = 0.5\,dB$	-20.0	0.24	-20.7	0.25	-18.3	0.14	-11.1	0.03	-7.2	0.01
$\sigma_{Mag} = 1\,dB$	-16.9	0.47	-17.4	0.49	-16.1	0.36	-10.6	0.09	-7.1	0.05

TABLE 5. NMSE error (closed surface) in presence of a Gaussian dispersion of the excitation profile phases (E-H-field synthesis filtered with threshold $10^{-3}\lambda_{max}$).

	$x_s = 0.5\lambda_0$		$x_s = \lambda_0$		$x_s = 2\lambda_0$		$x_s = 6\lambda_0$		$x_s = 10\lambda_0$	
	MV (dB)	SD (dB)	MV (dB)	SD (dB)	MV (dB)	SD (dB)	MV (dB)	SD (dB)	MV (dB)	SD (dB)
$\sigma_\phi = 0°$	-21.8	-	-22.8	-	-19.4	-	-11.2	-	-7.3	-
$\sigma_\phi = 2°$	-21.1	0.11	-21.9	0.11	-19.0	0.05	-11.2	0.01	-7.3	0.01
$\sigma_\phi = 5°$	-18.5	0.33	-19.0	0.35	-17.3	0.23	-10.9	0.05	-7.2	0.02

$E-$ or $H-$field based synthesis technique [see Eq. (6) for $E-$field synthesis] may be usefully employed [15]. Regarding the $E-$field based approach, comparison of the results reported in Table 3 with those in Tables 1 and 2 indicates that its performances approximate closely those observed using the $E-H$ synthesis technique regardless of the choice of closed or open synthesis surfaces, provided modal filtering is applied to the latter. Designers should be aware of these aspects when choosing a certain approach to near-field synthesis.

Finally, the robustness of the synthesis technique with respect to magnitude and phase variations introduced by the non-ideal behavior of phase shifters, attenuators, and amplifiers [19] used in the RF circuitry realizing the desired array excitation, was estimated. Tables 4 and 5 report computed figures for the *NMSE* mean (*MV*) and standard deviation (*SD*), for the $E-H$ synthesis technique with modal filtering, relative to several different synthesis planes upon assuming random Gaussian probabilistic distributions for magnitude and phase. Fifty Monte Carlo realizations were run for deriving each of several sets of results corresponding to respective magnitude variances $\sigma_{Mag} = 0.5dB$ and $\sigma_{Mag} = 1dB$, and respective phase variances $\sigma_\phi = 2°$ and $\sigma_\phi = 5°$, for the array excitations. The reported analysis generally reveals only a modest quality degradation, induced by the non-ideal behavior of the array feeding network, in the synthesized Bessel beams. Similar trends, which are not reported for the sake of brevity, were observed using the $E-$field based synthesis technique with modal filtering.

B. SYNTHESIS OF TILTED BESSEL BEAMS

Many practical applications may require steerable antenna beams to improve the detection accuracy of moving objects, to scan specific volumes (e.g., around body tumors), or beyond indoor obstacles (e.g., pillars, furnishings) [21]. For instance, one may desire to realize near field wireless links between pair of subarrays located on parallel planes in a multi-point to multi-point communication system (e.g., a wireless, reconfigurable, mobile data bus). In such a case, characterizing the synthesized wave-fields degradation along a chosen propagation path would be of key interest. The excitation profiles yielding the required beams would then be determined upon defining target fields on select synthesis surfaces on a $x = x_s$ plane parallel to the subarray. In Appendix A analytical expressions useful to derive Bessel beam target fields propagating along an arbitrary $\phi-$angle in the xy plane, are provided.

Figs. 6 and 7 show the spatial distribution of the electric field on the synthesis plane placed in $x_s = \lambda_0$ as well as on orthogonal planes to the propagation direction

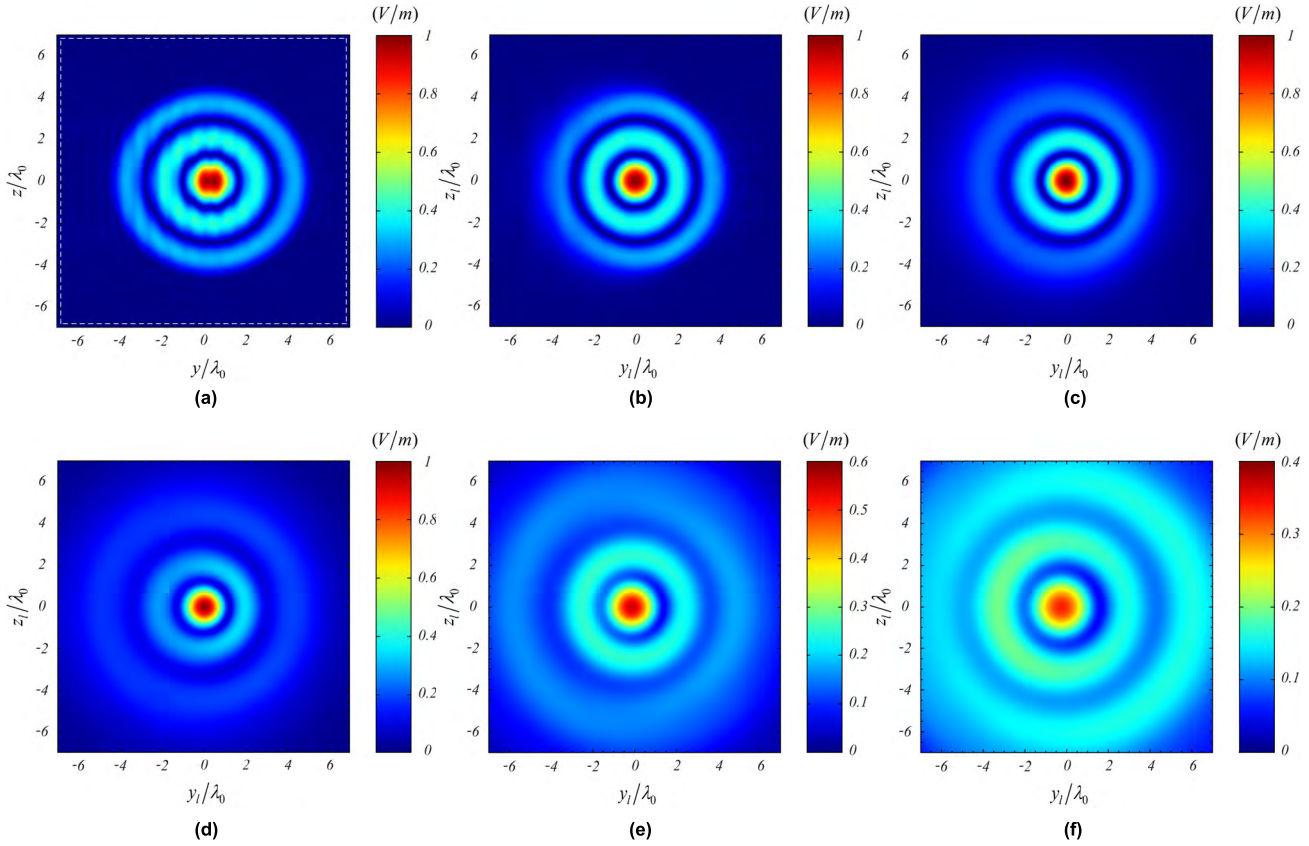

FIGURE 6. Spatial distribution of the electric field (z-component) of the Bessel beam (a) on the synthesis surface at $x_s = \lambda_0$, and along the propagation direction for $\phi = 20°$: (b) $\rho = 2\lambda_0$, (c) $\rho = 5\lambda_0$, (d) $\rho = 10\lambda_0$, (e) $\rho = 15\lambda_0$, and (f) $\rho = 20\lambda_0$. A gradual degradation of the Bessel beam is caused by diffractive processes as the radial observation distance increases.

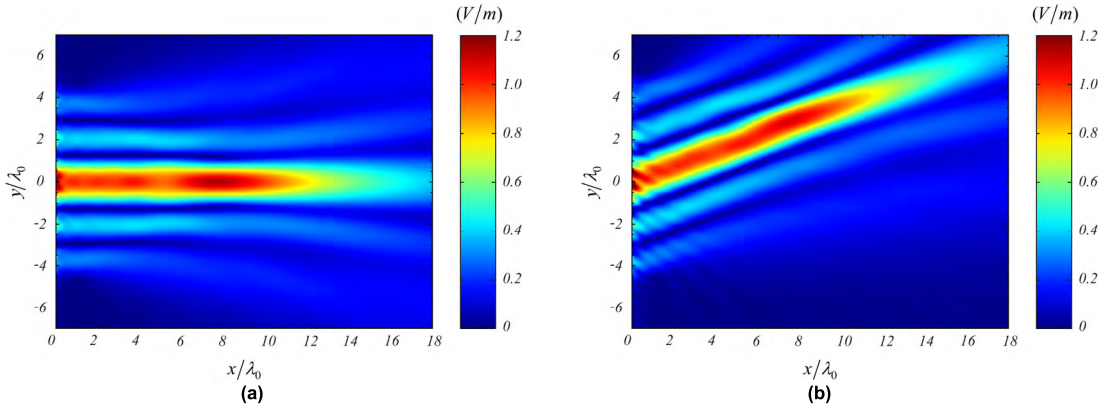

FIGURE 7. Spatial distribution of the electric field (z-component) of the Bessel beam for different tilt angles: (a) $\phi = 0°$, (b) $\phi = 20°$. An interference wave process, which can also be seen in Fig. 6a, is observed near the array when the tilt angle increases.

$\phi = 20°$. Accordingly, a tilted reference frame (y_l, z_l) centered about the $\rho-$axis was employed to plot the spatial distribution of the synthesized field at several distances along the $\rho-$axis. It may be appreciated that the Bessel beam substantially maintains its amplitude and shape up to about $\rho = 10\lambda_0$, then it starts degrading although the main beam is still circumferential even at $\rho = 20\lambda_0$. The main beam amplitude on the $\rho-$axis for different $\phi-$angles up to $\phi = 30°$ is reported in Fig. 8. It is worth observing that the spatial decay, after roughly $10\lambda_0$, features an initial rate that is larger than for spherical decay before settling to the spherical wave propagation regime at about $\rho \simeq 30\lambda_0$. Moreover, the main beam amplitude ripple remains fairly small up to about 10° beam tilt, then increasing